UNIVERSITY OF PATRAS
DEPARTMENT OF MECHANICAL ENGINEERING AND AERONAUTICS
DIVISION OF AERONAUTICAL ENGINEERING
LABORATORY OF APPLIED MECHANICS AND VIBRATIONS

MASTER THESIS

Drag coefficient analysis of satellites in Low Earth Orbits.

Nazlidou Panagiota

1059843

Vassilios Kostopoulos-Supervisor Professor

PATRAS, September/2023

The introductory part of this master thesis was carried out at the Zentrum fuer Telematik, Wuerzburg as part of my bachelor thesis while the computational part is solely research done at the university of Patras.

University of Patras, Mechanical Engineering and Aeronautics
Nazlidou Panagiota

Η έγκριση της διπλωματικής εργασίας δεν υποδηλοί την αποδοχή των γνωμών του συγγραφέα. Κατά τη συγγραφή τηρήθηκαν οι αρχές της ακαδημαϊκής δεοντολογίας.

ΠΕΡΙΛΗΨΗ

Υπολογισμός συντελεστή τριβής σε χαμηλή γήινη τροχιά

Ναζλίδου Παναγιώτα

Τις τελευταίες δεκαετίες, αυξημένο είναι το ενδιαφέρον της αεροδιαστημικής κοινότητας στις χαμηλές γήινες τροχιές. Χιλιάδες δορυφόροι εκτοξεύονται τα τελευταία χρόνια σε αυτά τα υψόμετρα εκμεταλλευόμενοι τα πολλά πλεονεκτήματα που αυτές οι τροχιές προσφέρουν. Ένα από τα σημαντικότερα πλεονεκτήματα ή μειονεκτήματα αυτών των τροχιών είναι η χαμηλή διάρκεια ζωής αυτών των δορυφόρων καθώς βρίσκονται σε περιβάλλον όπου η τριβή είναι αρκετά σημαντική λόγω την παρουσία του ατομικού οξυγόνου. Η τριβή, λοιπόν, είναι ένας παράγοντας που βοηθάει στο οι τροχιές να παραμένουν καθαρές αφού εξασφαλίζει την επιστροφή του δορυφόρου στην ατμόσφαιρα όπου καίγεται. Ωστόσο μπορεί να αποτελέσει καταστροφικό στοιχείο για μια αποστολή αν δεν υπολογιστεί σωστά. Σε αυτή τη διπλωματική, μελετάτε η τριβή ως φαινόμενο και μετέπειτα υπολογίζεται χρησιμοποιώντας το λογισμικό Moflow+. Για την χρήση του λογισμικού, περιγράφεται η διαδικασία συσχέτισης των Χαμηλών Γήινων Τροχιών με εφαρμογές κενού όπως αυτές που πραγματοποιούνται στο CERN. Αφού επιβεβαιωθούν οι συνθήκες της θερμόσφαιρας, υπολογίζεται ο συντελεστής τριβής σε μικροδορυφόρους.

Λέξεις κλειδιά: Συντελεστής τριβής, Χαμηλή Γήινη Τροχιά, Αραιή ατμόσφαιρα

ABSTRACT

Drag coefficient analysis of satellites in Low Earth Orbits

Panagiota Nazlidou

Within the past decades, very low Earth orbits (VLEO) have been of key interest for a variety of commercial space missions primarily focusing on Earth Observation and Telecommunications. Thousands of satellites have been launched at these altitudes the last few years, taking advantage of the thermospheric environment of these orbits. One of the main characteristics at these altitudes is the low lifespan the satellites due to the magnitude of the drag force as a result of increased atomic oxygen presence. Therefore, drag force takes important part in keeping these orbits clean since it ensures deorbiting of the satellites. However, it can be a disastrous element for a mission if it is not calculated correctly. On the course of this thesis, a review of the thermospheric environment takes place following by drag coefficient estimation using the Moflow+ software. The process of correlating Low Earth Orbits with vacuum applications is described to correctly represent the thermospheric environment. After confirming the conditions which best describe the simulation box as well as the satellite, the drag coefficient of various Cubesat satellites take place.

Keywords: Drag coefficient; ATOX; Rarefied Aerodynamics

TABLE OF FIGURES

LIST OF FIGURES

NOMENCLATURE

α_D (m/s^2) – drag deceleration

α (dimensionless) – accommodation coefficient

λ (m) – mean free path

ρ (kg/m^3) – atmospheric density

A (m^2) – ram area of the satellite

$A_{plan,k}$ (m^2) – surface area of the k^{th} panel

B (m^2/kg) – ballistic coefficient

C_D (dimensionless) – drag coefficient

$C_{D,k}$ (dimensionless) – drag coefficient of the k^{th} panel

E (cm) – Erosion depth

K_n (dimensionless) – Knudsen number

l_r (m) – characteristic length of the satellite

m (kg) – mass of the satellite

T_i (K) – kinetic temperature of an incoming molecule

T_r (K) – kinetic temperature of an outgoing molecule

T_w (K) – wall temperature of the satellite

V_{rel} (m/s) – relative velocity

Contents

ACKOWLEDGEMENTS

Throughout the writing of this thesis, I have received a great deal of support and assistance.

I would first like to gratefully acknowledge my supervisor Prof. Vassilis Kostopoulos from the University of Patras. Prof. Kostopoulos not only supported me since the first week of my university studies by giving me the opportunities to participate in Aerospace-related groups and projects, but he was always willing to help me with my academic decisions. I could never follow my passion for space if it were not for his contribution. I am grateful for his guidance and support on the course of my master thesis.

I would also like to express my gratitude towards my supervisor from CERN Jose Antonio Ferreira Somoza, my group leader Paolo Chiggiato and the developers of Molflow+ Ady Marton and Roberto Kersevan for all their guidance and assistance in familiarizing myself with Molflow+ software. They were always willing to explain how to appropriately use this software and they were constantly improving it by adding additional tools such as force calculation.

Finally, my deep and sincere gratitude to professors who helped me in the process of developing my career as well as my family and close friends for their continuous and unparalleled love, help and support. This thesis would not have been possible without their encouragement and stimulating discussions.

1.0 INTRODUCTION

Due to the thermospheric environment of VLEO, particles collide with the surfaces of a satellite which orbit in these altitudes. This residual atmosphere defines the energy transferred between a satellite and the space environment itself. This energy transfer depends on several parameters such as particle state and composition, gas-surface collision geometry, surface materials, spacecraft altitude and relative velocity [1]. One of the main constitutes of the upper atmosphere (thermosphere) is atomic oxygen as illustrated in Figure 1 and one of the most serious hazards for the spacecraft's material degradation which is an unavoidable factor for characterizing the energy and momentum transfer in the system spacecraft-upper atmosphere. It is evident that a scholastic characterization of the effect of atomic oxygen is required to calculate a more accurate drag coefficient.

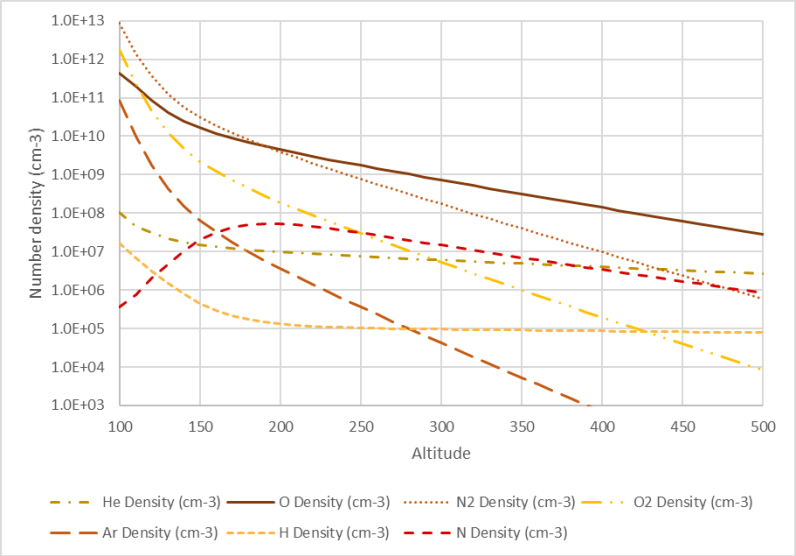

Figure 1: Number density of the atomic species in the VLEO environment

The most known orbital perturbations in VLEO, starting with the most influential across a wide range of altitudes, is the Earth gravity field accompanied by its irregularities perturbing and defining the satellites orbit. The J2 effect which describes the fluctuations of Earth's gravity field due to its oblateness is the most apparent perturbation orbital perturbation diverging from a typical point mass (Keplerian like) dynamic. Other gravity perturbations such as the third body attractions of other celestial bodies are much less dominant than the earth's divergent spherical harmonics. The solar radiation pressure seems to have little effect on typical satellite missions, as seen in Figure 2, however it also fluctuates depending on the solar cycle. In general, solar activity influences significantly the magnitude of atomic oxygen interactions with the spacecraft materials, consequently affecting the drag coefficient of the spacecraft. Thus, its influence must be carefully examined. What is worth mentioning in Figure 1 is the exponential increase of drag force in a logarithmic scale decrease of the altitude. All these perturbations affect the trajectory of the satellite as if they accelerate or decelerate it. We will mainly focus on the deceleration due to drag. [2] analyzes the accelerations and decelerations caused by the other perturbations.

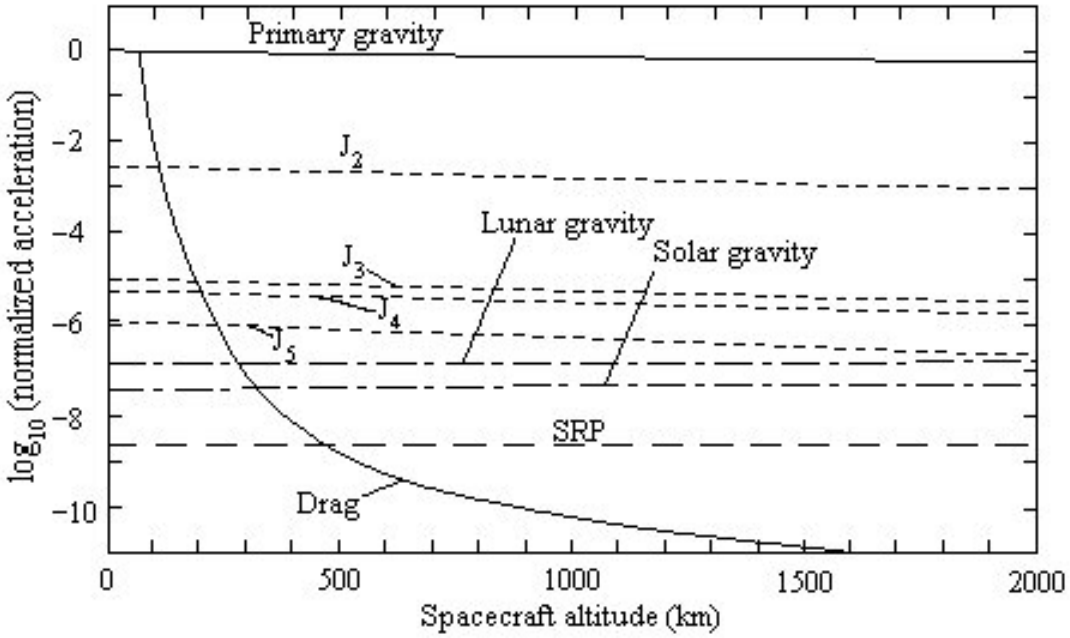

Figure 2: Comparison of different disturbing accelerations in LEO. Extracted from Ref. [3]

Despite drag being the most dominant force in VLEO, drag coefficient calculation with sufficient accuracy remains a challenging topic. Many theories have been developed to accurately calculate the drag coefficient but all of them are based on assumptions which decreases the final accuracy of the calculation. In addition, all these theories require information about the characteristics of space environment which can be extracted from thermospheric models. Uncertainties existing in the thermospheric models also contribute to the reduction of the total accuracy. Therefore, the computation of drag coefficient constitute a sophisticated problem which depends in several factors.

The essence of drag coefficient estimation is described by Equation 1, a relationship between drag deceleration and the drag experienced by the satellite:

$$a_D = -\frac{1}{2}\rho\frac{C_D A}{m}V_{rel}^2\overrightarrow{V_{rel}}$$

(1)

where a_D is the satellite deceleration, ρ is the atmospheric density, C_D is the drag coefficient, V_{rel} is the relative velocity and A the surface area facing the flow.

Assuming known drag acceleration obtained either though satellite accelerometers or through TLE data or paddlewheel satellites or in even more precise cases SLR data, this equation reveals a strong dependence between drag coefficient and atmospheric density. Evidently, satellite ram surface area and mass as well as the relative velocity are factors which effect the accuracy of the drag coefficient estimation. Thus, the calculation of the drag coefficient seems to be a very sophisticated topic let alone considering the difficulty of avoiding bias and errors. However, simplifications and assumptions are made to examine its correlation with the parameters which affect a satellite the most. For example, the relative velocity can be assumed a known/given quantity. We can make this assumption as the velocity of the satellite is determined through either orbit propagation and filtering or GNSS data while the winds are assumed to corotate with the Earth's atmosphere. Last assumption is the introduction of the inverse ballistic coefficient given by Equation 1 and Equation 2.

$$B = C_D A/m$$

(2)

By introducing the ballistic coefficient, the process of calculating the drag coefficient is simplified as we examine the effects of mass and surface area separately. Two ways of solving Equation 1 are identified (Figure 3). First, Equation 1 can be solved by using an atmospheric model

which gives us the atmospheric composition based on data bases but incorporating its bias and errors. This way we solve to the ballistic coefficient and then examine the effects of mass and surface area. Another method of solving Equation 1 is the implementation of a model based on gas surface interactions. Having calculated the drag coefficient, a comparison with the results derived with the first method can be made to validate the assumptions of the GSI model.

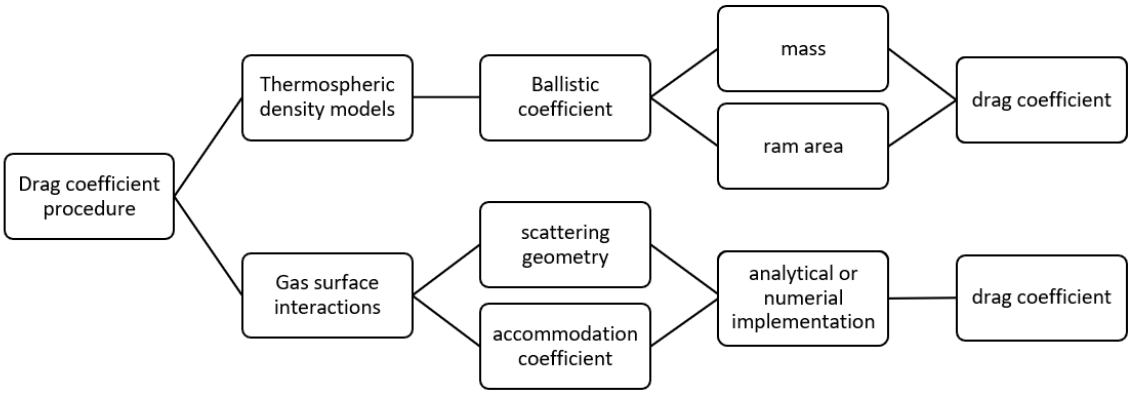

Figure 3: Different approaches of calculating the drag coefficient

In general, drag coefficient is a function of gas-surface interactions, satellite surface contamination and atmospheric composition. These parameters are dependent on each other thus the process of calculating the drag coefficient can be compared to a cycle transversal problem, something we should expect as building a satellite in an environment with atmosphere is similar to building an airplane or spaceplane. Assumptions are being made at the beginning of the procedure based on data and results from previous missions until a convergence to a solution is achieved.

For example, the density is being calculated based on the existed thermospheric models. After simulating the environment through a DSMC simulation an estimation of the density can

take place. If the result diverges from the one derived from the thermospheric model, then changes in the overall simulation or the thermospheric models should take place. However, additional empirical data are necessary to increase the accuracy. The satellite in-orbit can potentially measure the density of the thermosphere based on some instruments existing on-board. This value can therefore be compared with the one used in the thermospheric model or the one derived in the simulation. These data are useful to adjust thermospheric models and lead to a more accurate solutions of density estimations and therefore the drag coefficient.

2.0 VERY LOW EARTH ORBIT ENVIRONMENT

Having pointed out the effect of atmospheric density in the accurate calculation of drag coefficient and integrity of the satellite, the characterization of the rarefied environment is a key point of a satellite's orbital lifetime. As it not one of the primary goals of this report, a short introduction of this topic will take place.

Thermosphere is a high-altitude layer described by increasing density variations with altitude, solar flux and geomagnetic activity as seen in Figure 4. Evidently, the thermospheric density is immensely small compared to the altitudes of human transport flights, but it is a significant factor that decreases the orbital lifetime of a satellite. Being many orders lower in density leading to non-continuum flows, it requires a different approach to aerodynamics as will be discussed in the next chapter.

In general, the VLEO environment is dominated by gravity gradients, solar activity, and the earth's magnetic field. To describe the solar radiation and geomagnetic activity levels, the F10.7 and Ap indices are generally used. The F10.7 index describes the solar flux emitted at a wavelength of 10.7cm while the AP index is a measure of the variation of the magnetic field caused by irregular systems such solar radiation and interactions of the solar wind with the magnetosphere. These indices are later used as part of empirical atmospheric models which provide an estimation of the density given a specified location in space and time.

Examining the composition of the thermospheric density, it is observed that monoatomic oxygen is the main constitute of the residual atmosphere. In general, O2 is a very reactive gas itself. Monoatomic oxygen is far higher in reactivity resulting in unavoidable degradation with the

surfaces of the satellites. These defects can cause major failures in a satellite mission. Thus, satellite surfaces should have ATOX resistant properties and undergo thorough testing to atomic oxygen corrosion.

2.1 EMPIRICAL ATMOSPHERIC MODELS

Partial densities and subsequently the total density is a function of altitude under the influence of the solar cycle and geomagnetic activity. Several models have been developed to predict atmospheric characteristics at satellite altitudes and therefore to compute the aerodynamic drag, but NRLMSISE-00, DTM2000 and JB2006 are global references highly used due to their wide accessibility. All of them provide a density measurement for a wide range of altitudes and can be easily incorporated to open-source tools such as Orekit. Inputs of these models for predicting atmospheric characteristics are the F10.7 solar flux and A_p or K_p geomagnetic indices. The main practical difference between NRLMSISE-00, DTM2000 and JB2006 is that the NRLMSISE-00 and DTM2000 atmospheric models provide as outputs both total and partial densities while the JB2006 is used for calculating the total density itself.

It is recommended from the ECSS standard on Space environment to use the NRLMSISE-00 model for applications which require detailed composition of the atmosphere while the JB2008 for altitudes above 120 km [4]. According to [5], and restated from [6] the DTM2013, an advancement of DTM2000, becomes the most accurate model in the altitude range of 170 km to 275 km compared to the other mentioned empirical models.

Additional research points out the overall accuracy of DTM2013 under all conditions compared to NRLMSISE00 and JB2008 [5]. Specifically, in the 200-300 km altitude range the error of the DTM2013 atmospheric model varies between 5% and 10% [7]. Further improvement of the empirical DTM model results in higher accuracy such as the DTM2018 and DTM2020 models. The improvement of the DTM model is achieved by assimilating a more extensive database.

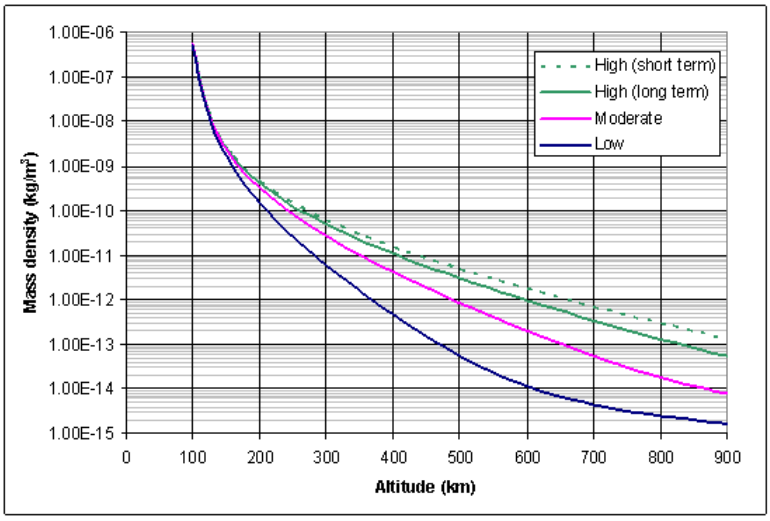

Figure 4: Variation of the mean air density with altitude for low, moderate, and high long and high short solar and geomagnetic activities as defined by JB2006 model. Extracted from Ref. [8]

2.2 CHARACTERIZATION OF THE FLOW

The density is not by itself alone an indicative factor describing the behavior of the rarefied environment. An entirely different approach to aerodynamics of a continuum regime has to be followed. Navier-Stokes' equations are no longer applicable to the flow at VLEO altitudes.

Therefore, the Knudsen number is used, able to classify the different flow regimes. This non-dimensional quantity is defined by Equation 3.

$$Kn = \lambda / l_r \quad (3)$$

where λ is the mean free path and l_r the characterizing length of the body.

The mean free path describes the collision-less distance of a molecule moving inside a regime and the characteristic length can be the length of the satellite parallel to the flow. By definition, a high Knudsen number (>10) indicates that molecules do not frequently collide with each other. However, the collisions between molecules and the surfaces of the satellites at high Knudsen numbers are of great significance. At these Knudsen numbers the flow is characterized as free molecular flow. For low such numbers, the mechanics of continuum flow regimes can be applied. A lower altitude bound of 130 km is given by [9].

For free molecular flows, another important quantity is the molecular speed. Molecular speed is a measure of the behavior of the flow. It can either behave as a collimated beam of molecules or as a chaotic drifting Maxwellian flow as seen in Figure 5. The former is defined as hyperthermal flow and the later hypothermal flow [10]. At hypothermal flow, all surfaces of the satellite may be impinged by molecules.

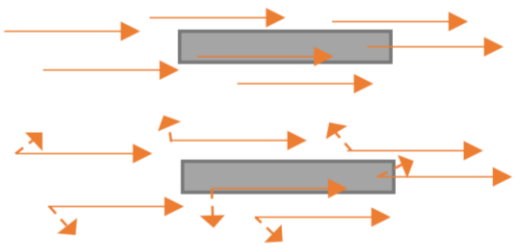

Figure 5: Hyperthermal and hypothermal flows

3.0 GAS SURFACE INTERACTIONS

At VLEO altitudes, the flow can be characterized as free molecular and hypothermal. The right definition of the flow is of great importance for the gas surface interaction modelling as they directly affect the angle of incidence, the interacting surfaces, and the frequency of collisions between the flow and these surfaces. Once a molecule interacts with the surface it will be either trapped or stick or scatter from it. Thus, incident and reflected velocities of these molecules must be calculated to model the exchange of energy and momentum due to impact and re emission. The process of modelling these interactions is the target of a Gas Surface Interaction Model (GSIM).

3.1 SCATTERING GEOMETRY

Starting with the calculation of the incidence velocity, a common approach widely used is the assumption of a Maxwellian distribution. Concerning the reflected velocity, several approaches have been developed based on different scattering geometric models. These scattering kernels, meaning the models which represent a specific reflected behavior, are illustrated in Figure 6. Moving from left to right, the reflected geometry can be diffusive, specular, a combination of diffusive and specular behavior as well as conical. Analytical approaches based on normal and tangential momentum transfer coefficients instead of scattering geometries have also been developed such as the model developed by Schaaf and Chambre. Such coefficients can be calculated experimentally without requiring the implementation of a scattering geometry.

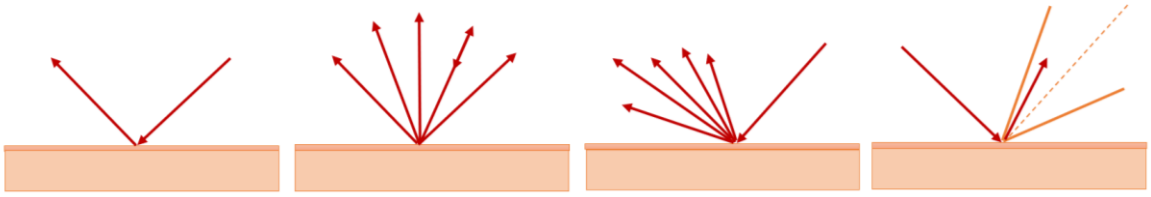

Figure 6: Scattering geometries: (a) diffuse reflection (b) specular reflection (c) mixed reflection (d) conical reflection

3.2 ACCOMMODATION COEFFICIENT

Even though these scattering geometries seem to be completely different, all of them require the specification of the same coefficient, the energy accommodation coefficient. This parameter is a non-dimensional physical quantity describing the behavior of particles in their collisions with a body or a surface Equation 4. The accommodation coefficient takes values between 0 and 1. Zero accommodation coefficient implies that there is no energy transfer and specular reflection exhibits while the complete case (accommodation coefficient equals 1) models the diffusive reflection. Respectively, a>0 means that quasi-specular reflection is observed.

$$\alpha = T_i - T_r/(T_i - T_w) \quad (4)$$

where Ti is the kinetic temperature of an incoming molecule, Tr is the kinetic temperature of the outgoing molecule and Tw is the temperature of the surface of the satellite (Mehta et al.-Drag coefficient modeling for grace using DSMC-finished).

Some worth-mentioning observations are that accommodation coefficients are nearly unity for very low mean altitudes and decrease with increasing mean altitude or low solar activity. Atomic oxygen increases the accommodation coefficient when absorbed while the absorption decreases with lower solar activity. Additionally, higher incident kinetic energies seem to increase the accommodation coefficient. Furthermore, night-time and day-time accommodation coefficients may differentiate [11]. Experiments on contaminated surfaces showed that the accommodation coefficient remains almost constant independently of the material (K. Moe and M.M. Moe 2011;Mostaza Prieto, Graziano, and Roberts 2014). Generally, the case of diffuse reemission with incomplete accommodation coefficient is broadly used for the altitudes operated by VLEO projects [9], [13].

3.3 GAS-SURAFCE INTERACTION MODELS

The scattering geometries together with the accommodation coefficient constitute the fundament of a GSIM model providing an estimation of the drag coefficient. Based on a different combination of these parameters or a different approach of implementing them, mathematical equations describing these GSI models are derived. The most common GSI models used in Direct Simulation Monte Carlo (DSMC) calculations will be described as it will be the main method of calculating the drag coefficient for this report.

3.3.1 Maxwell's model

Starting with the Maxwell model, it is the simplest GSI interaction model implementing both specular and diffuse reflections. This model is a probabilistic approach where the molecules scatter diffusively with probability Po and specularly with probability 1-Po [14]. The scattering kernel of Maxwell's model is described by the linear combination of the scattering kernel for diffuse and specular reflection. However, high-speed molecular experiments showed a more complex reflective behavior than the one resulting from the Maxwell's model [15].

3.3.2 CLL

A better probabilistic approach of the GSI models is the CLL method. This approach specifies independent scattering kernels for normal and tangential particle velocities. As a result, the CLL uses two accommodation coefficients, the normal and tangential momentum accommodation coefficients for describing the physics behind the reflection [16]. In contrast with Maxwell model, it has been shown to match the scattering distributions of certain molecular beam experiments [17].

3.3.3 Diffuse re-emission with incomplete accommodation coefficient.

In general, clean, and smooth surfaces exposed to freestream particles exhibit slightly more specular behavior (lower accommodation coefficient). However, due to the increased adsorption of atomic oxygen in VLEO, the surfaces are being contaminated and etched resulting in a more

diffusive behavior. Therefore, as the name of the model implies, the diffuse re-emission with incomplete accommodation coefficient model (DRIA) assumes that the particles are always re-emitted with a diffuse distribution, but their energy is not fully accommodated [18].

4.0 CALCULATION OF THE DRAG COEFFICIENT

4.1 ANALYTICAL METHODS

Having defined the mechanism which describes gas-surface interactions, the forces can therefore be calculated based on energy and momentum transfer. For approaches using normal and tangential momentum accommodation coefficients an analytical solution is derived directly without the need of modeling the scattered distribution [19]. However, angular (angle of incidence) dependence of normal and tangential momentum accommodation coefficient at a surface has been observed [19]. For example, the normal momentum accommodation coefficient is observed to decrease with increasing angle of incidence. In general, these coefficients are meant to be determined by experiments, but it is difficult to reproduce orbital conditions on Earth facilities [10].

Eventually, the analytical expressions for the calculation of the drag which are derived can be applied mostly in simplex geometries such as circles, plates, and cylinders.

4.2 NUMERICAL METHODS

For more complex geometries, the aerodynamics coefficients must be calculated by means of numeric methods. To elaborate this necessity, one can think of a simplex geometry which is divided into a finite number of plates. Each of these plates can be characterized as a convex shape

described by the analytical methods presented in the subchapter Analytical methods. All these plates-surfaces have their own orientation in space and the resulted force applied in each plate is different. Subsequently, the coefficient of each plate is different. Thus, the overall force coefficient of the body is found by summing up the contribution of every plate and dividing by the reference area. Examples of this mechanism are the following numerical methods: panel methods, Ray Tracing panel methods, Test Particle model Carlo methods and Direct simulation Monte Carlo methods. Hybrid methods combining two or more numerical methods have been developed to overcome disadvantages of one method and take the vantage points of the other.

4.2.1 Panel methods

To obtain the drag coefficient of an arbitrary shape, a panel method can be used. Established on the principle of finite elements, the drag coefficient of the entire body is calculated as follows:

$$C_D = \sum\left(C_{D,k} A_{plan,k}\right) / \sum\left(A_{plan,k}\right) \quad (5)$$

where $A_{plan,k}$ is the geometric area of the kth panel and $C_{D,k}$ is the drag coefficient of the panel facing the incoming flow as the flow is hyperthermal and treated as a collimated beam of molecules.

This approach is a simple numerical method applied to more complex but convex shapes as it does not encounter secondary reflections nor shadowing of concave geometries. To examine if an object is convex, research has been carried out by [20] introducing the convexity of a body

for different shapes and configurations as seen in Figure 7. The less convex a shape is, the less the accuracy of the drag coefficient estimation. Panel methods are often used as a reference of the efficiency of using a numerical method to a complex shape even though they are not complete accurate for complex non-convex geometries.

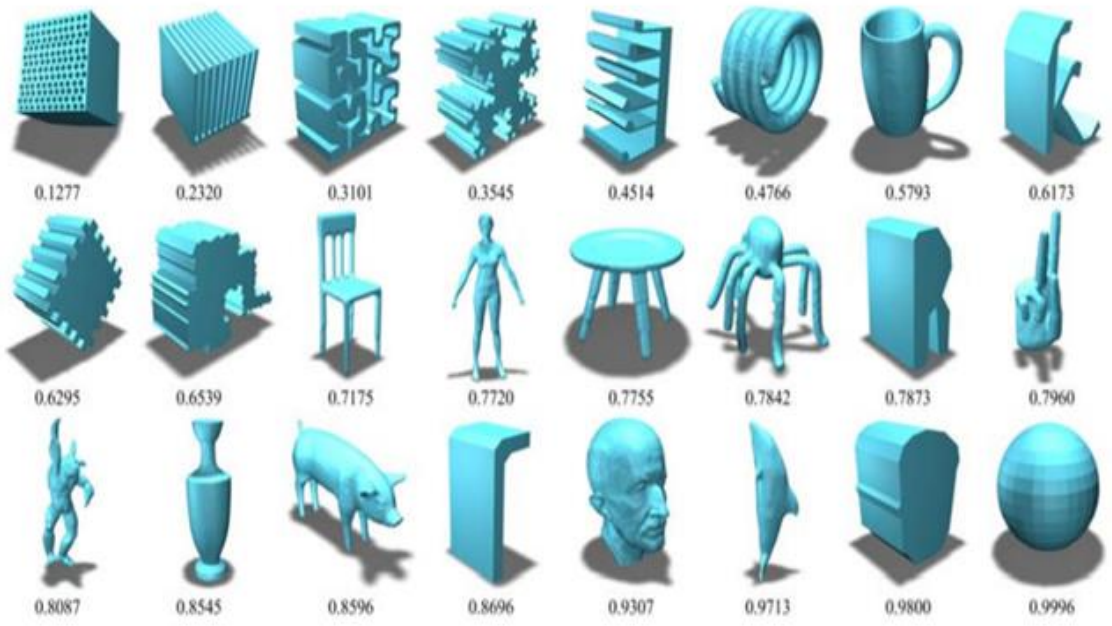

Figure 7: 3D shapes ranked by a convexity measure. Extracted from Ref. [20]

4.2.2 Ray tracing panel methods

Ray tracing panel method is an advancement of the panel method as it considers the shielding of the satellite surfaces. The difference between panel method and RTP method in practice is that the later extracts the shadowed panels from the calculation of the overall drag coefficient. However, it is only valid under hyperthermal conditions.

4.2.3 Test Particle Monte Carlo method

TPMC method goes a step further in respect to panel methods. It is consisted of a computational domain where particles represent a high number of real molecules. These particles are fired into the computational domain and either strike the surfaces of the satellite body or leave the computational domain. Each particle is sequentially fired into the computational domain, avoiding collisions between particles. Focusing on the particles and their behaviors/trajectories, the definition of a scattering kernel is unavoidable in contrast with panel methods which can be implemented with pressure and stress coefficients. The configuration of this method is seen in Figure 8.

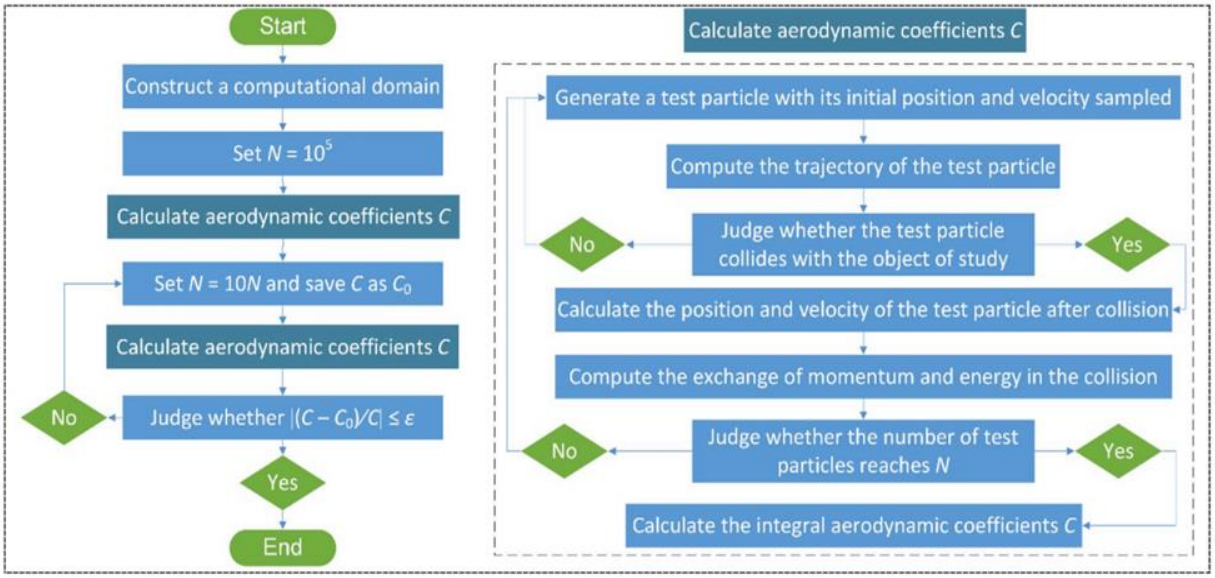

Figure 8: A Test Particle Monte Carlo Approach. Extracted from Ref**.** [21]

4.2.4 Direct Simulation Monte Carlo

Like TPMC, DSMC is a method consisted of a computational domain where an effective number of particles represents a specified number of real molecules. The difference between these two methods is that in DSMC the particles are fired simultaneously resulting in collisions between particles thus allowing for a wide range of applications. The process of a DSMC software is described in Figure 9 and provides the highest accuracy. However, the disadvantage of DSMC is the prohibitive computational time it requires as it takes time for the simulation to reach a steady state. After this steady state, the resulted flow properties are the ones should be considered.

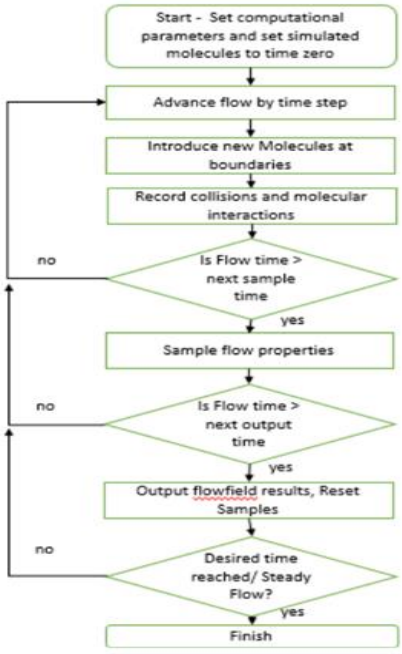

Figure 9: A Direct Simulation Monte Carlo flow diagram. Extracted from Ref. [22]

4.2.5 Hybrid methods

The Hybrid method which will be discussed is a combination of the Ray Tracing Panel method and the Test Particle Monte Carlo. The RTP method accounts for surface shielding but cannot model multiple reflections. If a geometry is convex then the possibility of a particle impacting to another surface is very low so the calculation of the drag coefficient will be sufficiently accurate if we only use the RTP method. However, if a geometry is complex then multiple reflections will happen. If these reflections are avoided, the estimation of the force and therefore of the drag coefficient could theoretically be underestimated resulting in decreased orbital lifetime but given the fact that collision behavior as witnessed empirically is highly diffusive (high accommodation coefficient values), the actual effect in orbit lifetime is marginal..

To compensate for the multiple reflections while keeping the computational time required low, a hybrid method of RTP and TPMC should be developed. For this scope, a simplified version of TPMC provides an estimation of the reflected free molecular flow which would be incident on a second surface. The simplification is based upon the principle of using the RTP method to define the incident molecular flux instead of firing particles into the computational domain. Then, the TPMC calculates the re-emitted particles which could impact a second surface.

4.2.6 Comparison of the numerical methods

Figure 10 compares and points out the features of the discussed methods. Starting with the panel method, it is recommended to be used at simple geometries such as spheres, cylinders, and plates. As the geometry becomes more complex but is still convex, RTP methods accounts for surface shielding providing higher accuracy. When surfaces have concaves, a hybrid method combining the vantage point of TPMC with RTP can be used offering high accuracy with less computational time requirements than TPMC. The only disadvantage of the hybrid method is that is unable to accurately model sub-hyperthermal flows in contrast with TPMC. The characteristic of the DSMC method which enables it to be valid for a wide range of altitudes is its ability to model collisions between molecules. Despite being its vantage point, collisions between molecules are the reason why this method is so computationally expensive.

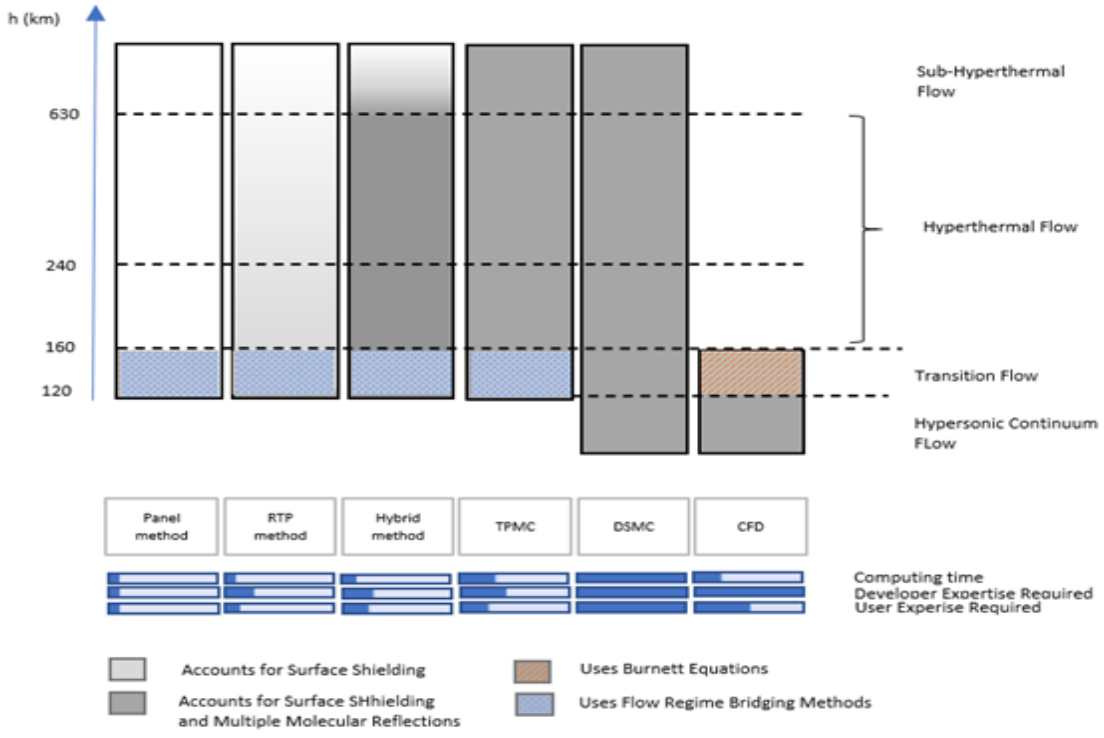

Figure 10: A comparison of the numerical methods concerning their capabilities and requirements.

Reproduced from Ref. [10] to include Hybrid methods

5.0 SIMULATION OF DRAG COEFFICIENT

5.1 APPROACH

For the calculation of the drag coefficient of Cubesat platforms in altitudes of 500 km, the Test Particle Monte Carlo (TPMC) approach is decided to be used. As discussed in the Subchapter "4.2.6 Comparison of Numerical Methods", the TPMC approach provides very efficient results in Free Molecular Flows while reducing the computational time. The software which is used for our simulations is Molflow+: A free molecular flow software simulating the pressure when Ultra-High vacuum conditions are met. To give a deeper understanding of the procedure to the reader, a quick introduction and correlation of Very Low Earth Orbits with vacuum conditions is briefly analyzed.

5.2 VACUUM TECHNOLOGY AND VERY LOW EARTH ORBITS.

After I finished my work at the Zentrum fuer Telematiks in Gemrany where I was using the DSMC approach for calculating the drag coefficient due to the accuracy prerequisite of the project I was working, I got an internship at CERN at a vacuum technology position. The vacuum applications which they implement at CERN are highly related with behaviours in Very Low Earth Orbits which I found very captivating.

My first day at CERN my supervisor asked me out of curiosity what the pressure in my simulations of the drag coefficient for an altitude of 250 km was. I did not realise how crucial this question was as I never gave a pressure value to any of my scripts for the DSMC simulation in the SPARTA software. In my scripts, I defined pretty much everything except the pressure. That's because the vacuum can be defined by a combination of other quantities as well. In vacuum applications the pressure is the most important value to be defined as it indicates the vacuum conditions which have been achieved within the machines. Thus, in terms of pressure the different degrees of vacuum and their pressure boundaries are defined in the Table 1 [Chiggiato- Vacuum Technology for Ion sources]. For the purposes of this thesis, we will mostly consider High and Ultra high vacuum conditions. [Handbook of vacuum science and technology].

Table 1: Different degrees of vacuum and their pressure boundaries

	Pressure boundaries (mbar)	Pressure Boundaries (Pa)
Low Vacuum (LV)	1000-1	1e5 to 1e2
Medium Vacuum (MV)	1 to 10e-3	1e2 to 1e-1
High Vacuum (HV)	1e-3 to 1e-9	1e-1 to 1e-7
Ultra-high vacuum (UHV)	1e-9 to 1e-12	1e-7 to 1e-10
Extreme vacuum (XHV)	<1e-12	<1e-10

In addition, the ideal-gas equation of state from statistical considerations may be rewritten in terms of the total number of molecules N in the gas [Vacuum Technology for Ion sources], as seen in Equation 6.

$$\boldsymbol{PV = Nk_bT} \quad \textbf{(6)}$$

Where k_b is the Boltzmann constant (1.38e-23 J/K), P the gas pressure, T the temperature and V the volume. Calculating to N/V which is the number density we can define the number of molecules per cm3 for the different pressure range.

The Knudsen number which was introduced earlier in the subchapter "2.2 Characterization of the flow" is proportional to the mean free path and the characteristic length of the body. The mean free path describes the collision-less distance of a molecule moving inside a regime and the characteristic length can be the length of the satellite parallel to the flow.

The mean free path λ is inversely proportional to the number density $n = P/(k_b T)$ and the collision cross-section s_c.

$$\boldsymbol{\lambda = \frac{1}{sqrt(2) n s_c}} \quad \textbf{(7)}$$

For free molecular flows, another important quantity is the molecular speed as discussed in the introduction of the chapter "Calculation of drag coefficient". The molecular speed can be calculated based on the Equation 8.

$$\boldsymbol{v_{mol} = \sqrt{\frac{8RT}{p_i M}}} \quad \textbf{(8)}$$

Where T is the Temperature of the environment and M the molar mass.

This equation could be used individually for each element with molar mass M or by calculating an average of the molar mass of the thermospheric environment. This would help us with faster computational times in terms of using Molflow+ which will be described later. If for accuracy reasons the velocity is calculated individually then multiple simulation s is Molflow+ must be done and the sum up of the forces will give the result of the drag coefficient. Assuming

that the particles are corotating with the Earth atmosphere then the molecular flow is summing up with the velocity of the satellite.

The average Molar Mass is calculated based on the Equation 9.

$$\boldsymbol{M = \sum x_i * M_i} \quad \textbf{(9)}$$

Where xi is the fraction of the gas species in the thermosphere and Mi their molar mass.

The velocity of the satellite is calculated based on the orbital elements which continuously describe its orbit. In the simulations of this thesis, circular orbits are assumed to easily simulate the drag coefficient of the satellite using Molflow+. Thus, the equation which best describes the velocity of a satellite in a specific orbit is given by:

$$\boldsymbol{vsat = \sqrt{\frac{GM_{central}}{R}}} \quad \textbf{(10)}$$

Where G is the universal gravitational constant, $M_{central}$ is the mass of the central body and R is the radius of orbit for the satellite.

Eventually the relative velocity is described by the summing up of the satellite V_{sat} and the molecular speed v_{mol} as given in equation 11. Depending on the rotation of the satellite in relation to Earth's rotation, the velocities are being added or extracted.

$$\boldsymbol{\overline{v_{rel}} = \overline{v_{mol}} + \overline{v_{sat}}} \quad \textbf{(11)}$$

For elliptic orbits, the environment changes continuously requiring the integration of scripts to simulate this changing behaviour, which is far beyond the purpose of this thesis. However, if the reader is interested in examining this behaviour, I would suggest that they use Python in corporation with the Orekit Libraries- A space flight dynamics library to simulate the

environment. This would require the integration of Molflow+ software inside the code to continuously run simulations for every timestep which would probably be challenging.

In Molflow there is a relatively new addition of calculating the forces which is very convenient timewise. However, Moflow is developed based on vacuum applications. For vacuum applications the most important quantities are the outgassing rate and the sticking coefficient. Based on these values, the pressure distribution along the vacuum machine is calculated. The approach so far for the drag coefficient calculation is based on the number density of the thermospheric or the velocity and the direction of the particles relatively to the satellite. Thus, these quantities must be translated to outgassing rates and sticking coefficients to derive the forces and therefore drag coefficient.

My assumption of the difference is described in the Figures below. The left picture describes how Molflow is used in vacuum machines. In this case, the machine is system with specified limits within which the particles collide with the surface, and either is being absorbed by the surface or by a pump. In this system, the outgassing of the material is specified through experimentation and the pressure is calculated based on the properties of the machine.

The right picture depicts a satellite in thermospheric environment. The “machine” in this case is a system-to -be-defined by the user, and specifically a box which encloses the satellite. The dimensions of this box are defined by the user and directly affect the result of the simulation. The particles in this case collide with the satellite and if not absorbed, they are disappearing from the system. Measurements of the pressure and density of the thermosphere from previous satellite mission help to eventually calculate the pressure on the satellite surfaces and therefore the drag coefficient. So, in the first case the pressure is calculated based on the outgassing rate and in the

second case the pressure on the satellite surface is calculated based on the pressure and speed of the particles which practically is the same.

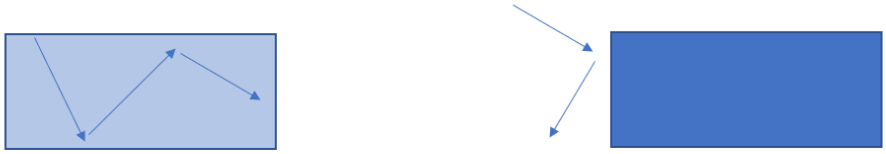

Figure 11: The main difference between vacuum applications (Left) and satellite drag coefficient applications (Right).

So, the outgassing rate of the "thermospheric environment" can be calculated based on the most important equation of vacuum applications.

$$\boldsymbol{Q = PV} \tag{12}$$

Where P is the pressure and V is the molecular speed distribution. All this theory will be better understood after being implemented in Molflow+. The new version of Molflow+ is implementing also the accommodation coefficient values of the satellite surfaces as well as the mode of reflection which are very useful for the drag coefficient calculation.

5.3 MOLFLOW+ SIMULATIONS

5.3.1 Geometrical configurations

For the purpose of this thesis, software freely available to students was used. The 3D design of the satellites was done in Spaceclaim which is a tool available in the student version of Ansys. To carry out the simulations in Molflow+, a STL file in ASCII format is required. However, the student version of Ansys does not provide the option to export as STL format in the Spaceclaim toolbox. To export the file as STL, the cad configuration must be inserted in the Mechanical toolbox of Ansys where it is being meshed by the user. After defining the mesh and changing the STL format to ASCII, the mesh can be exported as STL format. I would advise to not spend a lot of time meshing the cad configuration as it is later being processed automatically in Molflow+. For questions concerning the designing process of a satellite and its environment in Spaceclaim, the reader is encouraged to contact me for further information.

5.3.2 Definition of the environment

The most critical part of the drag coefficient estimation is to define the environment correctly. Thus, it is important to understand how to describe the thermospheric environment as a vacuum system to derive the results which we expect. The validation process of the assumptions made in the previous chapter consists of the GRACE satellite drag coefficient estimation in a 500 km altitude and comparison with the results derived from [22].

The dimensions of GRACE used for the simulations are given in Figure 12 and 13. Both figures were taken from [22].

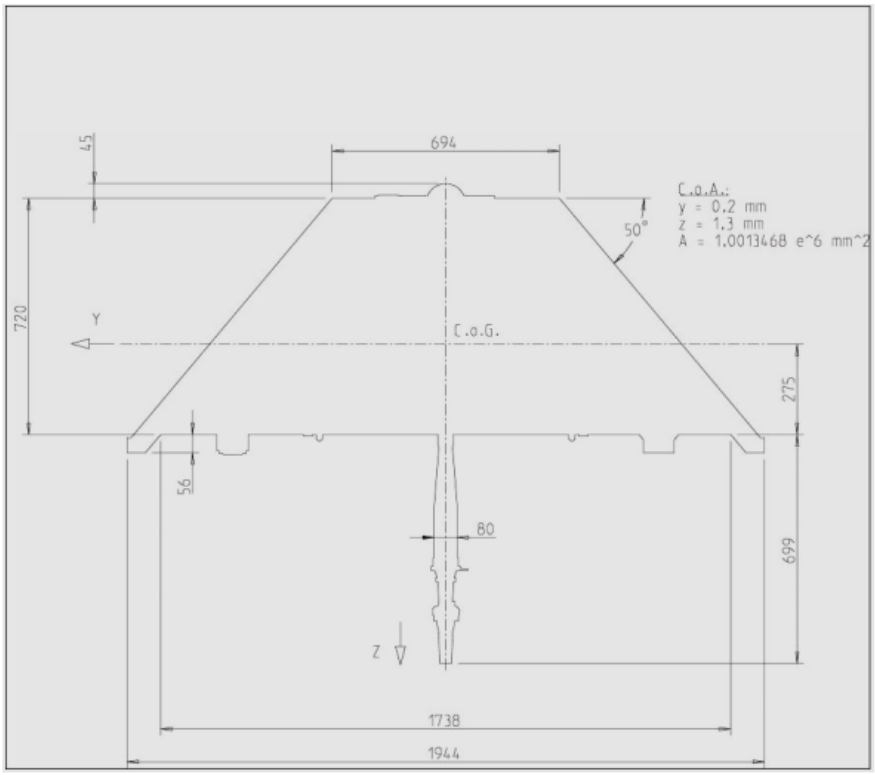

Figure 12: Front on view of GRACE satellite derived from [22].

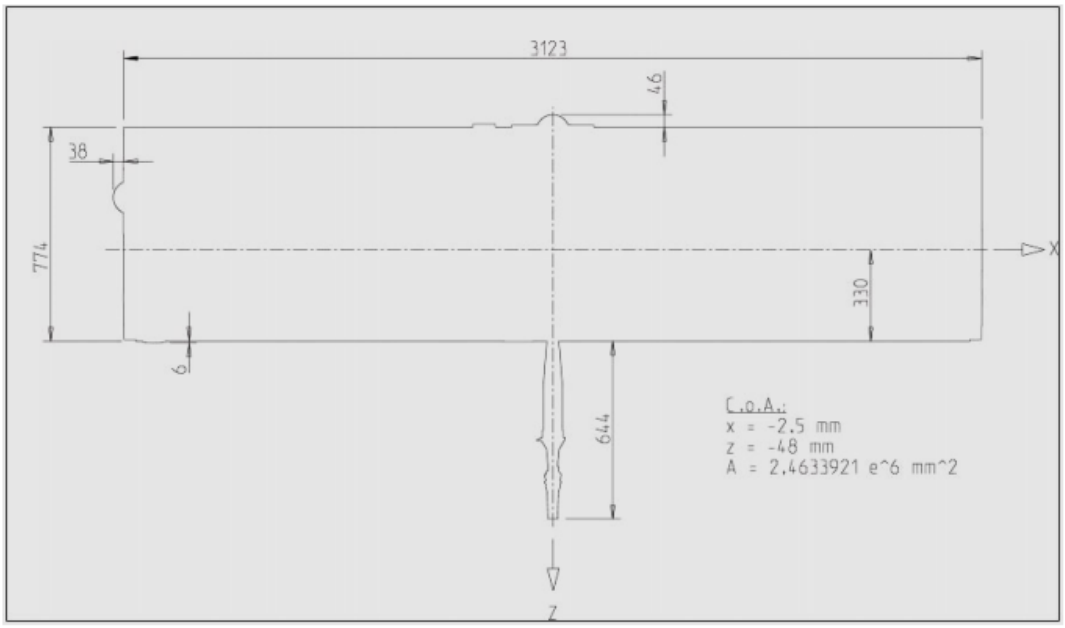

Figure 13: Side on view of GRACE satellite derived from [22].

The respective cad configuration in Spaceclaim is shown in Figure 14. The satellite is enclosed by a volume which represents the thermospheric environment. We need the box to define the outgassing coming out of the respective surfaces. The dimensions of the box can be calculated based on the following source Francis end Garcia-1997-The direct simulation monte carlo method.

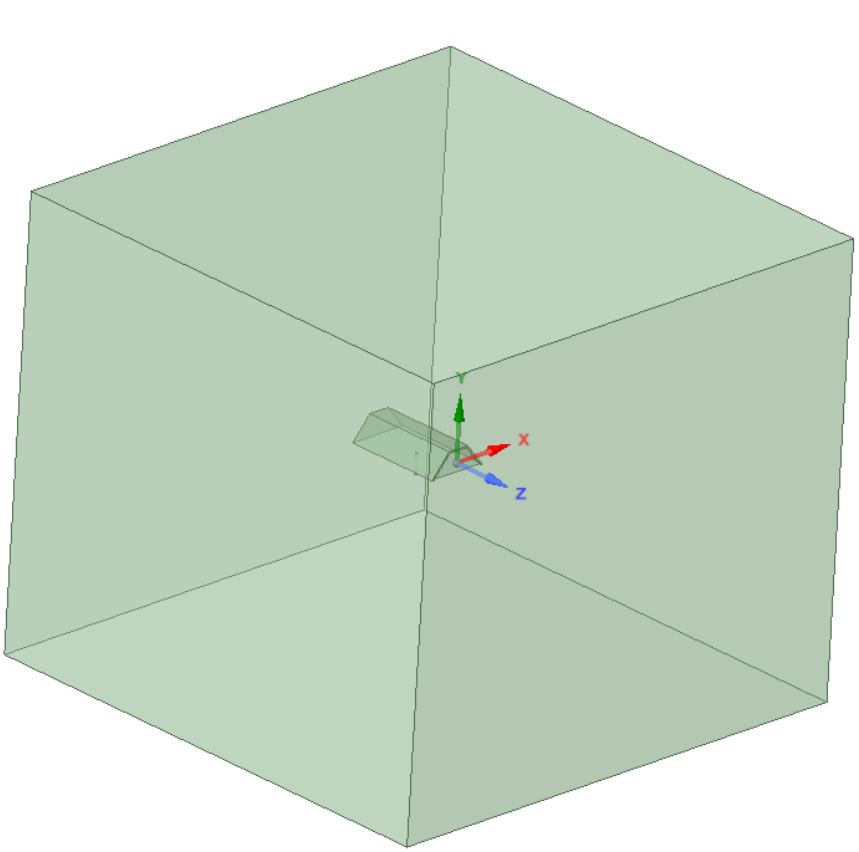

Figure 14: Representation of GRACE satellite and the thermospheric environment in Spaceclaim.

For quick meshing, the “Generate” tool in the Mechanical toolbox of Ansys was used. After exporting the mesh in STL format and importing it in Molflow+, the Mesh is being simplified by using the “Collapse” settings which automatically pop up when inserting the STL file as seen in Figure 15.

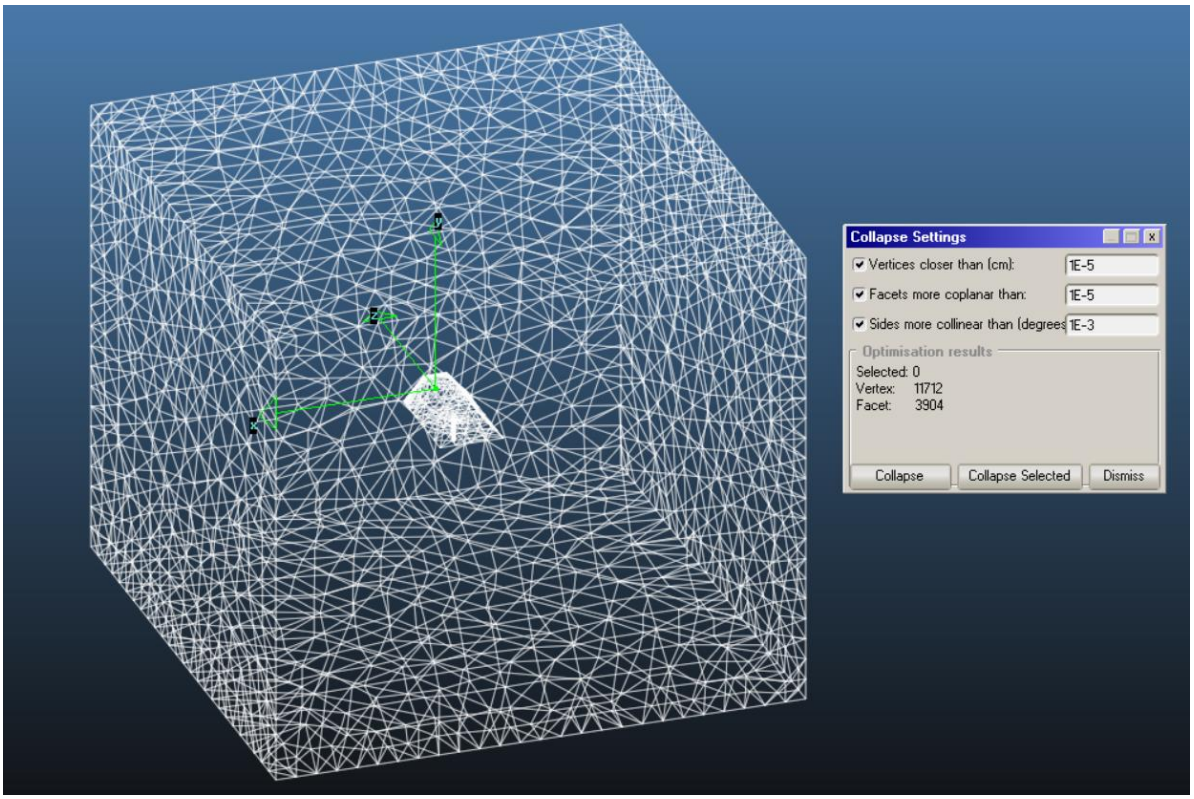

Figure 15: The mesh generated in Mechanical Ansys toolbox and inserted in Molflow+. The picture represents the mesh before collapsing it.

After using the “Collapse” setting the mesh is being simplified significantly, which makes the computational times to decrease. The collapsed STL file is illustrated in Figure 16. It is easily observable that the number of facets has decreased significantly.

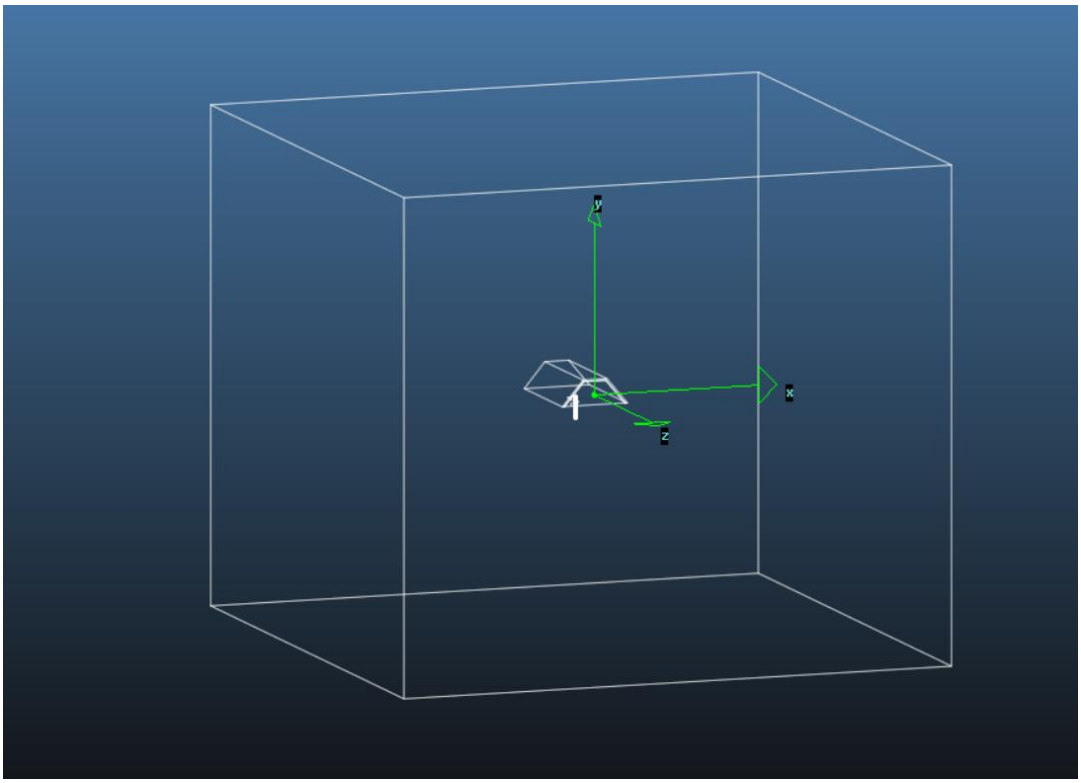

Figure 16: Mesh of the cad configuration after collapsing in Molflow+.

The geometry of the environment as well as the satellite have been defined perfectly. Next step, the most important and interesting one, is to define the properties of the thermospheric environment and the behaviour of the satellite in respect to the flow.

Molflow+ gives the option to categorize facets in groups. This tool is very convenient to distinguish the satellite facets as one selection and the thermospheric environment as a different selection. This helps the user to categorize groups of facets with the same properties, for example, the satellite surfaces as seen in Figure 17. The reader is encouraged to watch the Molflow webinar by Marton Ady to familiarize with those tools so that they are used efficiently.

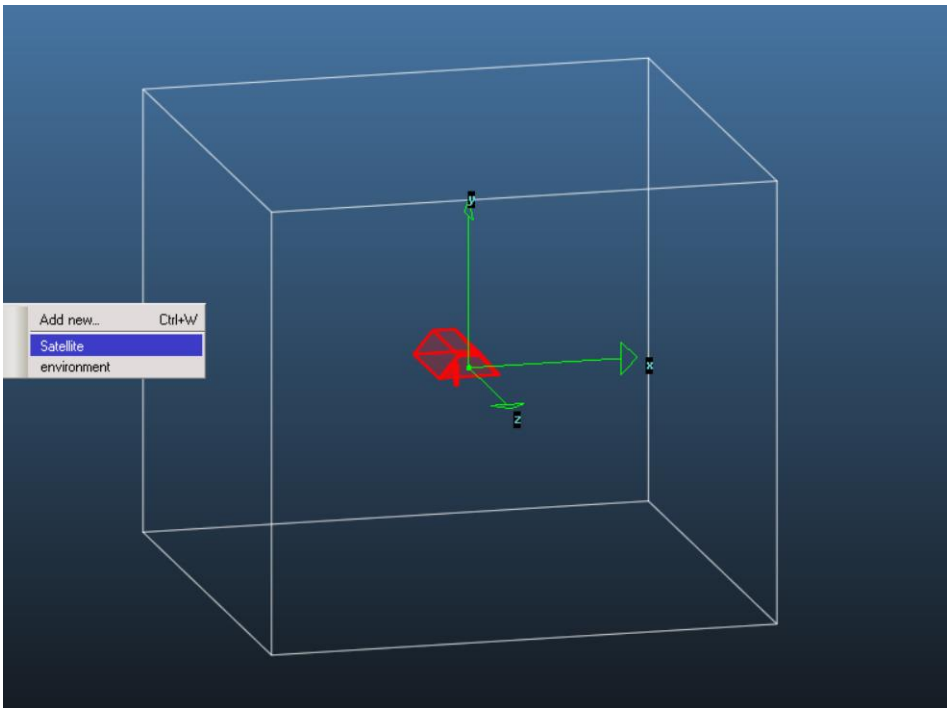

Figure 17: Defining selections within Molflow+ to categorize facets with same properties.

For the definition of the environment, the values for altitude, pressure, molecular mass and density, were derived from the Standard Atmosphere [reference. The values used for the altitude of 500 km are shown in Table 2. This quantities result in Outgassing rate of 3.63e-7 mbarl/s/cm2.

Table 2: Values used for simulation the thermospheric environment in 500 km altitude.

Parameter	Units	Values
Temperature	K	999.24
Density	Kgm-3	4.45e-13
Pressure	mbar	3,02e-9
Molecular weight	Kg/kmol	14,7
Molecular speed	m/s	1220

In addition to these values, the outgassing rate is being calculated based on the molecular speed and pressure which results in 3,6e-7 mbar/s/cm2. The desorption of the molecules is considered cosine, and the outgassing is being applied to the frontal facet, sides facets as well as the bottom facet. The upper facet is considered to be non-outgassing as the density decreases with increasing altitude and the molecules are moving from the denser to the sparser environments. In the exiting facet there is no outgassing as the satellite travels faster than the molecules. All the facets which describe the thermospheric environment are set to sticking factor equal to 1 which means that if the molecules come in contact with those facets, then they disappear. New molecules are constantly entering the computational domain from the outgassing facets.

After defining the thermospheric environment, the satellite movement as well as the properties of the satellite facets must be defined. Molflow+ allows to give speed to moving entities as seen in Figure 18. The satellite is moving in direction z with a velocity of 7611 m/s. The equation for calculating the velocity was given in Chapter 5.2. The “moving parts” setting must therefore be applied to the satellite selection of facets. This is done by the “Advanced facet parameters” setting as seen in Figure 19. The accommodation coefficient is set to 0.95.

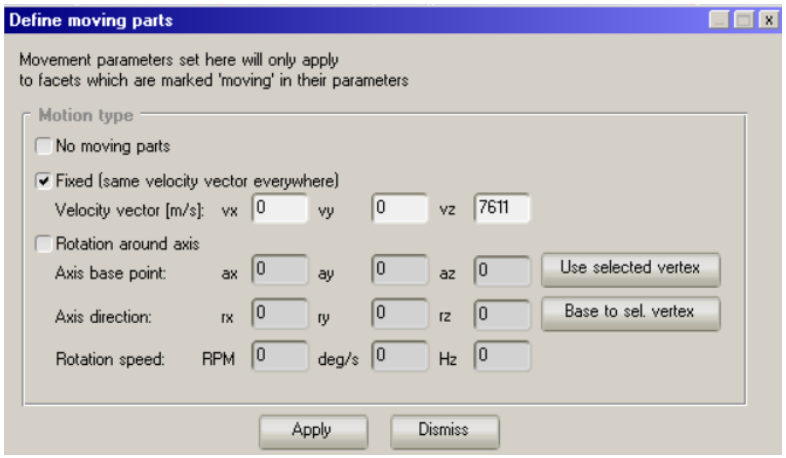

Figure 18: Defining the velocity (magnitude and direction) of the moving parts which in our case is the satellite orbital velocity.

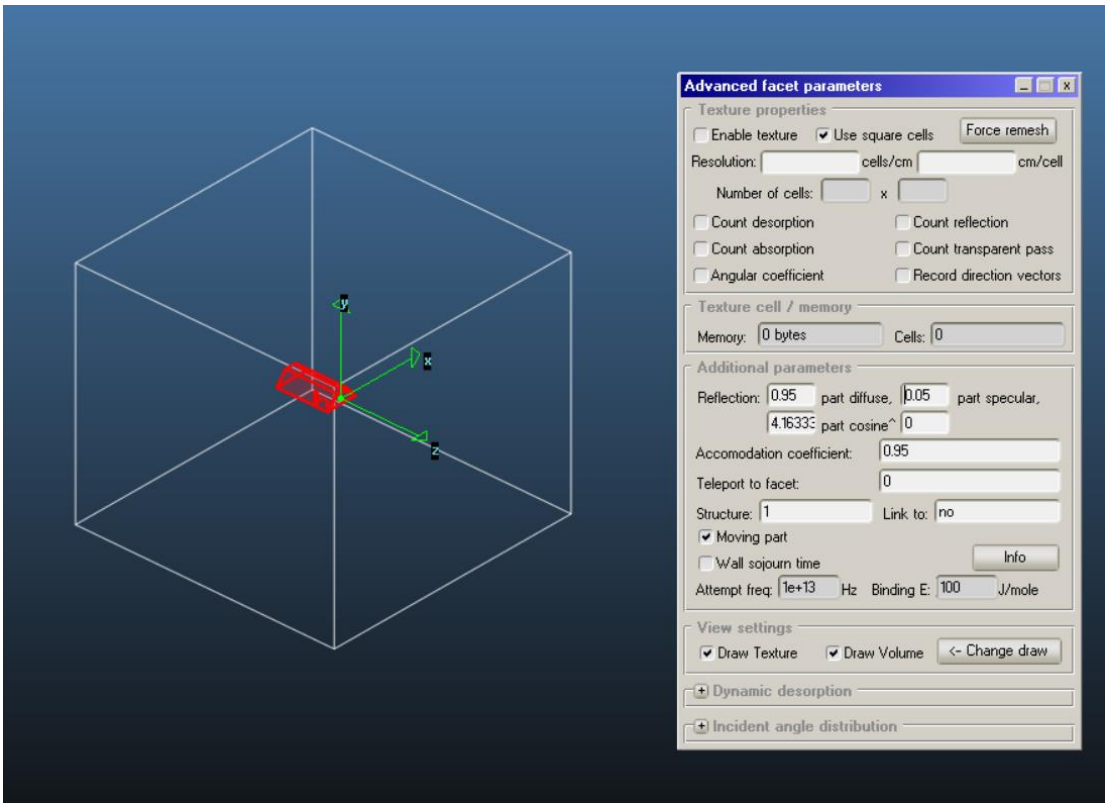

Figure 19: Defining the properties of the satellite. Specifically, assigning the velocities to its facets as well as the accommodation coefficient value.

Last step before running the simulation is to enable force measurement. As discussed earlier, for vacuum applications the most important quantity is Pressure thus the forces are not of high essence. Molflow+ is becoming a very useful tool for VLEO orbits, so the owners added the "Measure forces" tool to help aerospace industry with calculating directly the forces through Molflow+. However, as this tool is not used by everyone and it increases the computational cost of the simulation, it must be enabled by the individual who are interested in using it as seen in Figure 20.

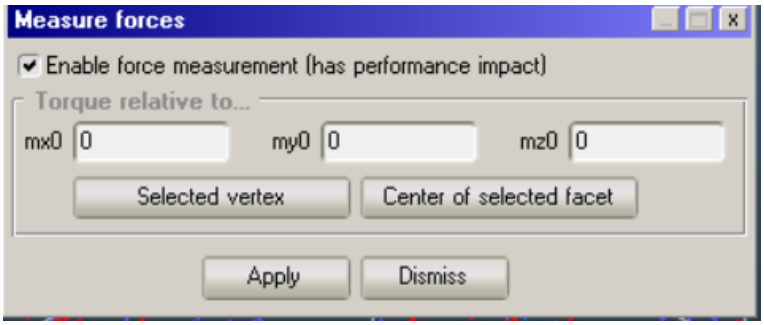

Figure 20: Enabling forces measurement in Molflow+.

Everything is now set up so the simulation can start. After letting the simulation to run for a while to obtain a stable result, the force value in Z axis which represents the drag force is being calculated. To calculate the force in Z, X or Y axis, the formula editor is used as seen in Figure 21.

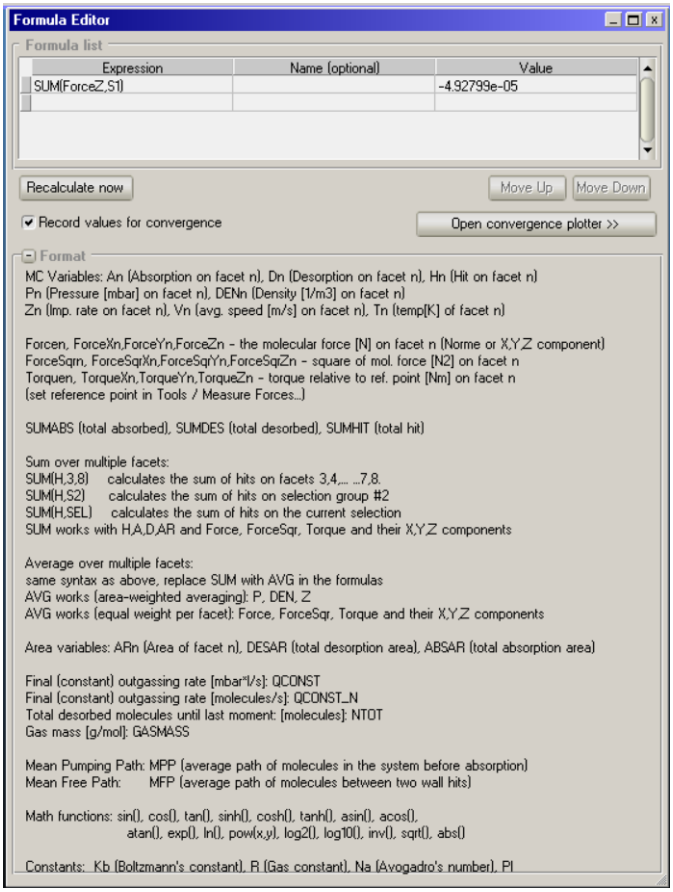

Figure 21: Formula editor for calculating the drag force in Z axis.

Based on this result and Equation 1, the drag coefficient is calculated. The results are given and being compared to the ones derived from Bullard in Table 3.

Table 3: Comparison of Moflow+ results with drag coefficient derived from [22].

Parameter	Molflow+ simulation	Bullard
Drag force (N)	4.93e-5	4.94e-5
Drag coefficient	3.1	3.16

For the calculation of the drag coefficient the same values with Bullard were used to compare if the result would be the same. The velocity which was used was the one derived directly

from the orbit of the satellite, as used by Bullard. The explanation which I could give for this example is that the outgassing is happening from multiple facets with a cosine distribution so that the actual relative speed in z axis approximates the orbital velocity of the satellite. The convergence of the results is a good indicator that the environment has been defined correctly.

5.3.3 Drag coefficient estimation of various CubeSat Platforms

At this chapter, the estimation of the drag coefficient of various CubeSat platforms take place. Specifically, the various sizes under examination are: 2U, 3U, 6U and 6U with deployed solar panels. The geometric configuration used for the simulations are shown in Figure 22.

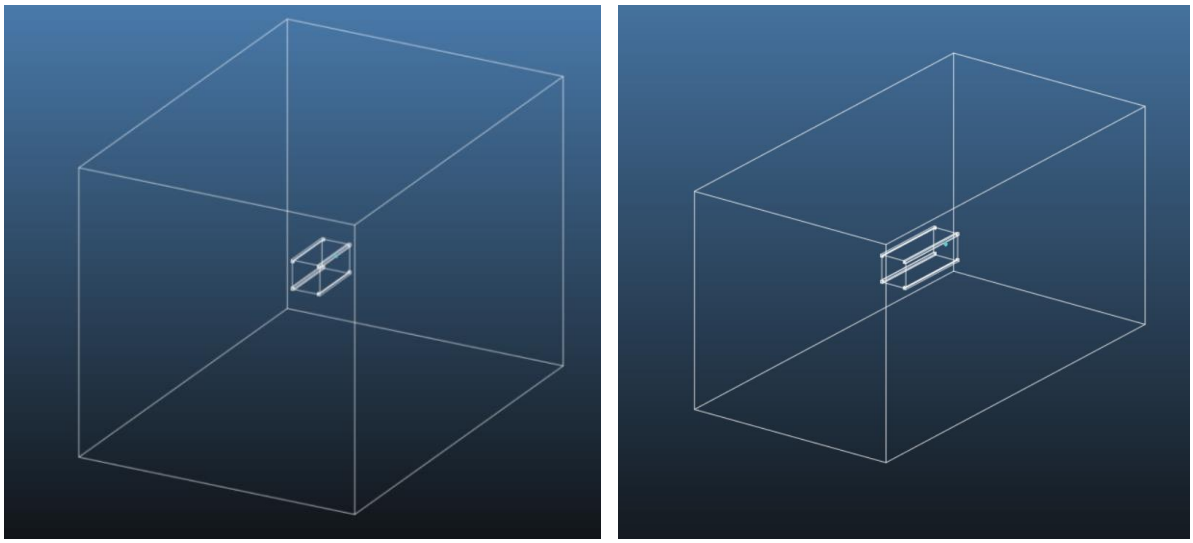

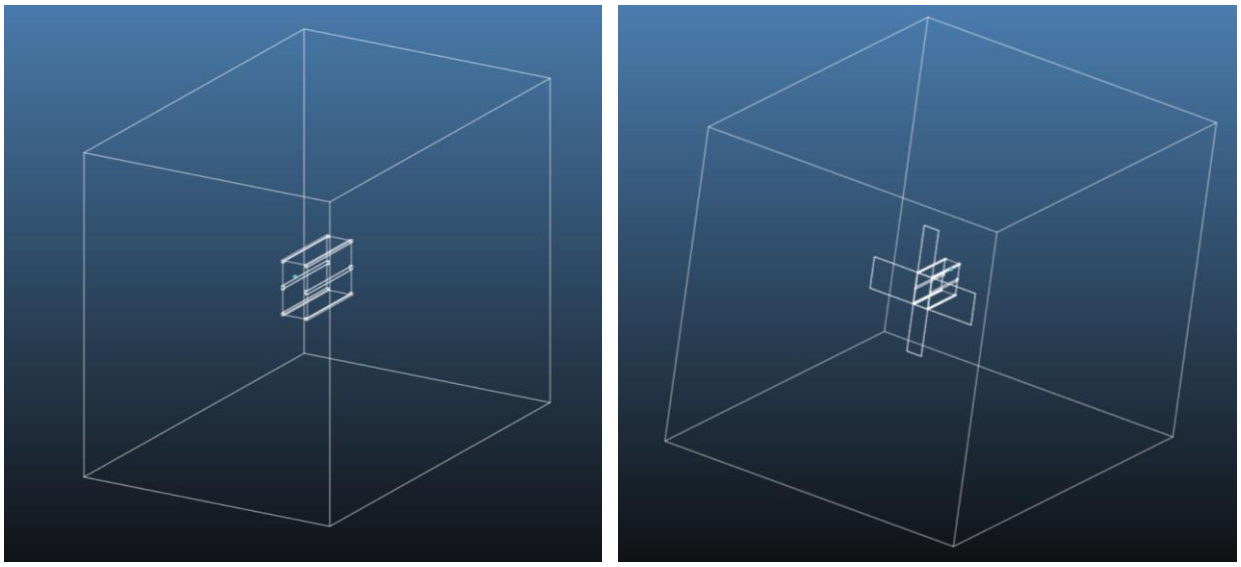

Figure 22: 2U CubeSat (Top Left), 3U CubeSat (Top Right), 6U CubeSat (Bottom Left) and 6U CubeSat with deployed panels (Bottom Right).

The results of the simulations are given in Table 4. Although the drag force acting on the satellite increases, the drag coefficient decreases due to the increased frontal surface area. It is observable that the 2U CubeSat does not experience a lot of drag force due to the very small length of the satellite. By increasing the length, (3U CubeSat) the drag force increases significantly. After doubling the frontal facet and keeping the length the same (from 3U to 6U Cubesat), the drag force is increased but it is noticeable that the increase in length had a more remarkable increase in drag force than the increase in frontal area.

Table 4: Molflow+ simulations for different CubeSat scenarios.

CubeSat	Force (N)	Drag Coefficient
2U	9.47e-9	0.06
3U	4.08e-7	2.64
6U	5.97e-7	1.93
6U with deployed solar panels	1.5e-6	0.54

6.0 ATOMIC OXYGEN CORROSION

It is of high importance in LEO environment to consider the presence of atomic oxygen. In general, atomic oxygen in LEO is formed by photodissociation of diatomic oxygen (Banks et al 2004). Being the main constitute of the residual atmosphere and highly corrosive, the collisions of it with the spacecraft surfaces initiates numerous chemical and physical such as elastic scattering, scattering with partial or full thermal accommodation [23] events. This way it does not only affect the thermal, mechanical, and optical properties of the exposed materials due to material loss and general degradation which is formed but the orbit of the satellite. As the altitude of the satellite decreases so is the atomic oxygen prevalence and the diffusive behavior of the overall reflecting particles and therefore the drag coefficient. The dependence of the drag force to the reflecting behaviour of the particles and therefore the presence of atomic oxygen indicates a correlation between the experienced drag and the atomic oxygen composition. This factor is generally encompassed and correlated to the overall accommodation coefficient in the gas/surface simulations.

The accommodation coefficient can be parameterized by three main factors as stated by (Pilinski, 2011). The three factors mentioned by Pilinski are the atomic oxygen pressure along the orbit, the mean molecular mass, and the relative velocity. The relative velocity is then used to calculate the kinetic energy which is essential for the calculation of the Langmuir parameter. The Langmuir parameter together with the atomic oxygen pressure are used to calculate the fraction of

surface covered by atomic oxygen. The resulting accommodation coefficient can be therefore used to calculate the drag coefficient within a numerical software implementation.

6.1 DEGRADATION OF MATERIALS DUE TO ATOMIC OXYGEN

An important measurement of the atomic oxygen degradation is the erosion depth. The erosion depth is a tool for material engineers to calculate degradation. It describes the depth to which the material is affected, and it is measured in length units. The erosion depth is directly proportional to the fluence of atomic oxygen and the erosion yield of the material.

$$E = Fluence\ x\ Erosion\ Yield$$

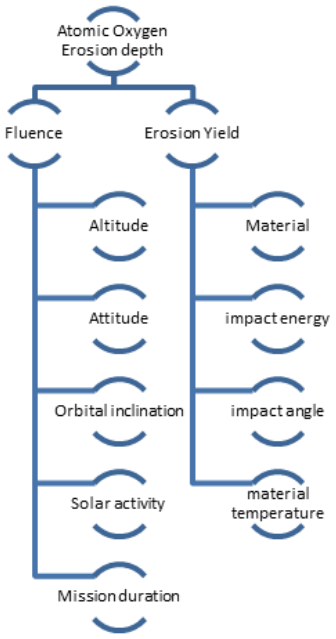

Figure 23: Erosion depth as a function of fluence and erosion yield

The fluence is the integral over time of the flux of AO crossing the surface [24]. Several factors affect the degree of degradation due to AO fluence, such as altitude, solar activity, orbital inclination, attitude, and mission duration [25]. Concerning erosion yield, it is a measurement of the volumetric loss per incident oxygen atom [25] It depends strongly on the material for example polymers are very susceptible to erosion yield thus having higher erosion yield, on the impact angle and in some cases on the material temperature [https://www.spenvis.oma.be/help/background/atmosphere/erosion.html]. The dependence of erosion yield on the impact energy [26] of the AO must be investigated in orbit.

General observations exist for the influence of various factors. Since the degree of surface degradation is directly proportional to AO fluence, when solar radiation activity increases (solar maximum) or the altitude of the spacecraft decreases, the population of AO increases and therefore the degradation. In addition, increase of the AO populations takes place with increased orbital inclination. Concerning the mission duration, the longer the mission the higher the exposure in AO [25].

Since absolute protection from ATOX erosion is not possible, techniques to mitigate the effect of ATOX in spacecrafts surfaces which are susceptible have been developed. These techniques consist of the development of materials with improved durability to ATOX, as well as the application of thin film protective coatings [27]. In general, the protection of the spacecraft should be optimized for the operating environment of the planned mission with an extra operating margin to allow for unpredictable variations in the orbital conditions or modifications of the

mission [25]. Therefore, the methods to calculate AO effect for a specific mission can be investigated.

Nevertheless, being affected by many factors which are not always accurately predictable, for example in-orbit resulting state transitions through mission operations and the actual solar activity experienced, it is difficult to practically predict the flux and therefore the fluence and the erosion yield of spacecraft materials without a wide margin for error reserved.

6.2 CALCULATION OF EROSION DEPTH

As mentioned earlier, the degradation of a spacecraft material to AO is described by the following equation $E = Fluence\ x\ Erosion\ Yield$.

6.2.1 Fluence

6.2.1.1 Tables

To calculate the fluence several ways are identified with different levels of accuracy. An initial estimation of the fluence could be derived using figures of flux as a function of the altitude or/and the solar activity such as figure x. Having defined the altitude of the satellite, one can easily estimate the fluence by assuming constant flux over time and multiple it with the duration of the mission. An example is given.

$$fluence = 1.1 * 10^{15} \frac{atoms}{cm^2 s} * 6months * 29 \frac{days}{month} * 24 \frac{hours}{day} * 60 \frac{min}{hour} * 60 \frac{sec}{min}$$

$$fluence\ of\ CubeSat = 1.7 * 10^{22} \frac{atoms}{cm^2}$$

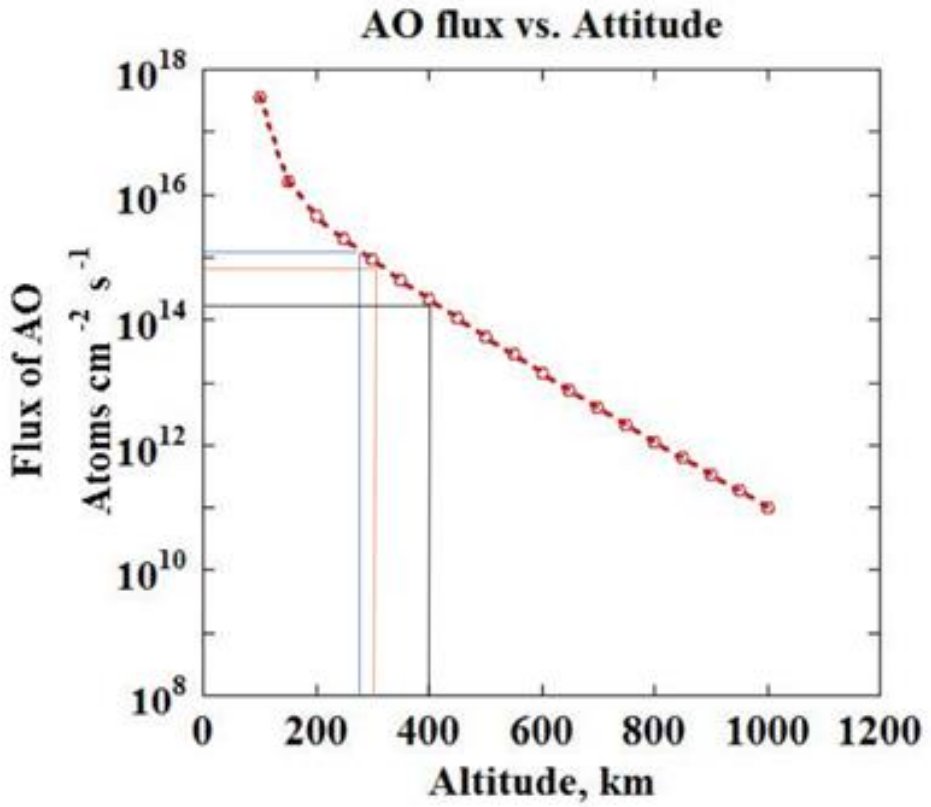

Figure 24: Flux of AO as a function of altitude. Extracted from [28].

6.2.1.2 Software

For higher accuracy, the software SPENVIS developed by ESA could be used which calculates the fluence based on the NRLMSISE-00 density model and the $F_{10.7}$, A_p *indices*. Within the model, it is possible to calculate not only the front fluence which the satellite experiences but

also the back fluence. Although the frontal surfaces are exposed to the most intense erosion hazard the back surfaces should be examined carefully if an organic material is used. Interestingly, based on an observation of the protective coatings which were used in the ISS solar arrays and a Monte Carlo simulation, it is highly recommended to use protective coatings only in one side of the material under protection. This is because if defects exist in the protective coatings, then the atomic oxygen may become trapped between the coating increasing the reactions of it with the material under protection. Thus, if there is a hazard to AO in the back of the satellites, a careful choice of the material should be done.

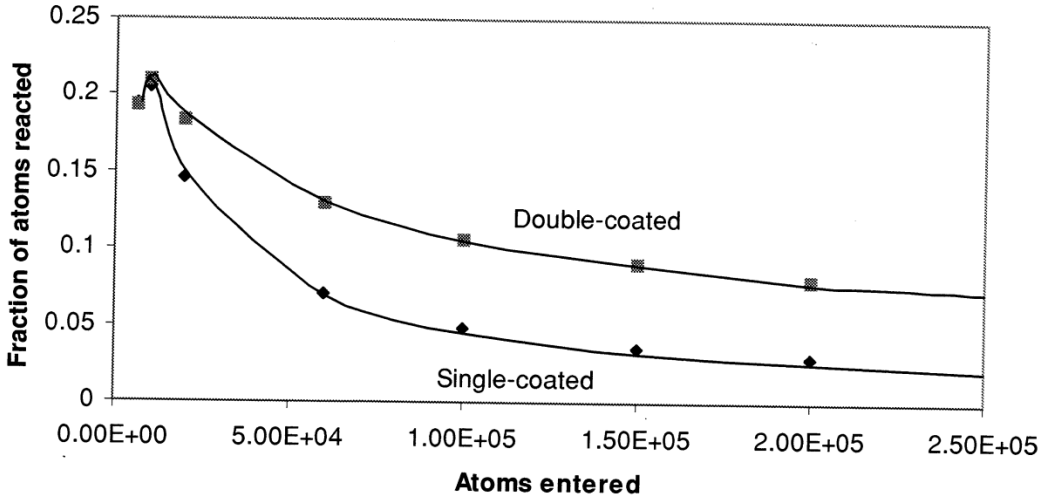

Figure 25: Monte Carlo computational atomic oxygen erosion predictions for sweeping incidence atomic oxygen attack at crack or scratch defect sites in the aluminized Kapton as a function of atomic oxygen fluence [29]

6.2.2 Erosion yield

The erosion yield depends strongly in the properties and chemical composition of the material as the difference between materials is often remarkable. Some general observations have been made based on experiments carried out in space and in ground-testing facilities to examine the yield of different materials.

6.2.2.1 General observations

Starting with the most vulnerable materials, polymers and organic materials which only contain carbon, hydrogen, oxygen, or nitrogen result in erosion yield which varies from $1\ to\ 4 * 10^{-24}\ \frac{cm^3}{atom}$. Less susceptible are the metallic materials except silver and osmium as they do not show macroscopic changes. Their erosion yield values are of the order of $10^{-26}\ \frac{cm^3}{atom}$. Silver and osmium are often assumed unacceptable for such use due to their low resistance to atomic oxygen. Nonmetallic materials such as silicon oxides, magnesium fluoride and aluminum oxides vary from $0.4\ to\ 2.8 * 10^{-28}\ \frac{cm^3}{atom}$ [25].

6.2.2.2 Tables

To obtain the erosion yield of different materials, tables summarizing these values have been constructed based on experiments performed in-orbit and evaluated in ground testing facilities. Some of them can be found in the following papers [25], [30]. An example is given in Table 1.

Table 5: Overview of AO reaction efficiencies of polymer films on several flights. Reproduced from [25]

Sample	**STS-5**	**STS 41-G**	**LDEF**	**STS-46**	**PPPL**	**MSFC**
Halar (bulk)		1.0-2.0	2.1	2.0-2.5	3.0-3.4	0.014-0.034
Lexan®		1.3-3.6		3.6-4.0		
PEEK(bulk)		4.7	2.3	2.0-4.0		
Tefzel		0.2		~1.0	2.8-3.0	0.11-0.12
Kapton® HN		3.3		3.3-4.3		
Kapton® H	3.0			3.5-3.9		
Black Kapton®				2.1-2.7	3.4	
TFE	<0.05		0.2	0.049-0.080		
FEP	<0.05	3.1-2.4	0.35	0.082	5.9-6.6	0.023

6.2.2.3 Analytical expressions

For polymers an analytical predictive erosion yield equation is presented in the following paper [30]. This equation was derived based on forty material samples which were exposed on the Low Earth Orbit environment on the exterior of the ISS for 4 years and has a high correlation coefficient (0.895) with these data. Therefore, the erosion yield to be calculated is a function of the number of atoms, bonds, or physical characteristics of the polymer as well as the fluence of atomic oxygen.

6.2.2.4 Software

Similar to calculating the fluence of atomic oxygen using SPENVIS, the software package incorporates the erosion yield of a variety of materials. However, there are materials not incorporated in the packages. It should be considered that the software package incorporates erosion yields of materials based on experiments carried out under specific environmental conditions. So, they incorporate their bias and errors.

7.0 CONCLUSIONS

The simulation of the aerodynamic forces is a very challenging topic as it depends on several factors which affect the final accuracy of the simulation. The accurate representation of the Very Low Earth Orbital Environment where the satellite orbits as well as the thorough understanding of the gas-surface interactions between the particles and the satellite are critical factors for the calculation of the aerodynamic coefficients.

Depending on the orbit of the satellite the number of the particles change, so does the interactions between particles and the surfaces. A very important quantity which must be considered on the course of the simulation is the atomic oxygen existing in the VLEO environment. The atomic oxygen is the reason the particle reflections become more diffusive as the surfaces of the satellite are being contaminated by atomic oxygen. This behaviour is described by the accommodation coefficient which indicates if the overall interacting particles reflect demonstrate a higher degree of diffusive behaviour.

The software used for simulating the interaction between the thermospheric environment and the satellite itself was Molflow+. Even though this software was initially developed for vacuum applications, the software has been upgraded to include force measurement in satellite facets. This provides the aerospace industry with a very efficient and fast software tool to calculate the drag force and therefore drag coefficient.

The procedure of simulating the environment is described thoroughly so that the reader has a greater understanding of how to calculate the drag coefficient efficiently. The thermospheric

conditions are being verified by comparing the results from Molflow+ for the GRACE satellite with the results derived from [22]. The results are in close agreement which verify the assumptions which have been made on the course of this thesis. After ensuring the convergence of the results, the drag coefficient of various Cubesat platforms is being calculated.

BIBLIOGRAPHY

[1] P. M. Mehta, C. A. McLaughlin, and E. K. Sutton, "Drag coefficient modeling for grace using Direct Simulation Monte Carlo," *Advances in Space Research*, vol. 52, no. 12, pp. 2035–2051, Dec. 2013, doi: 10.1016/j.asr.2013.08.033.

[2] W. ¨ Urzburg Luleå, F. Kunzi, O. Ruf, J. Scharnagl, K. Schilling, and M. Milz, "Development and Testing of a GPS-based Navigation System for Nanosatellites Statutory Declaration Title: Development and Testing of a GPS-based Navigation System for Nanosatellites," 2018.

[3] J. Virgili-Llop, "Spacecraft Flight in the Atmosphere," 2014, doi: 10.13140/RG.2.1.5192.8480.

[4] "Space engineering Space environment ECSS Secretariat ESA-ESTEC Requirements & Standards Division Noordwijk, The Netherlands," 2020.

[5] S. Bruinsma, "The DTM-2013 thermosphere model," *Journal of Space Weather and Space Climate*, vol. 5, 2014, doi: 10.1051/swsc/2015001.

[6] Y. Yang *et al.*, "Comparison of atmospheric mass density models using 1 a new data source: COSMIC satellite ephemerides", doi: 10.1002/essoar.10502170.1.

[7] D. R. Jackson *et al.*, "The Space Weather Atmosphere Models and Indices (SWAMI) project: Overview and first results," *Journal of Space Weather and Space Climate*, vol. 10, 2020, doi: 10.1051/swsc/2020019.

[8] "SPENVIS." https://www.spenvis.oma.be/ecss/e_st_10_04c/ecss_18_10_01.htm (accessed Feb. 24, 2022).

[9] N. H. Crisp *et al.*, “In-Orbit Aerodynamic Coefficient Measurements using SOAR (Satellite for Orbital Aerodynamics Research),” Dec. 2020, doi: 10.1016/j.actaastro.2020.12.024.

[10] D. Mostaza Prieto, B. P. Graziano, and P. C. E. Roberts, “Spacecraft drag modelling,” *Progress in Aerospace Sciences*, vol. 64. Elsevier Ltd, pp. 56–65, 2014. doi: 10.1016/j.paerosci.2013.09.001.

[11] M. D. Pilinksi, “CU Scholar Dynamic Gas-Surface Interaction Modeling for Satellite Aerodynamic Computations,” 2011. [Online]. Available: http://scholar.colorado.edu/asen_gradetds

[12] K. Moe and M.M. Moe, “Gas-Surface Interactions in Low-Earth Orbit,” in *American Institute of Physics Conference Series*, 2011, pp. 1313–1318.

[13] M. M. Moe, S. D. Wallace, and K. Moe, “Refinements in determining satellite drag coefficients - Method for resolving density discrepancies,” *Journal of Guidance, Control, and Dynamics*, vol. 16, no. 3, pp. 441–445, 1993, doi: 10.2514/3.21029.

[14] D. C. Wadsworth, “Gas-Surface Interaction Model Evaluation for DSMC Applications,” Jun. 2003, pp. 965–972. doi: 10.1063/1.1581644.

[15] J. F. Padilla, “ASSESSMENT OF GAS-SURFACE INTERACTION MODELS FOR COMPUTATION OF RAREFIED HYPERSONIC FLOWS,” 2008.

[16] P. M. Mehta, A. Walker, C. A. McLaughlin, and J. Koller, “Comparing physical drag coefficients computed using different gas-surface interaction models,” *Journal of Spacecraft and Rockets*, vol. 51, no. 3, pp. 873–883, 2014, doi: 10.2514/1.A32566.

[17] C. Cercignani and M. Lampis, “Kinetic models for gas—surface interactions,” *Transport Theory and Statistical Physics*, vol. 1, no. 2, pp. 101–114, Jan. 1971, doi: 10.1080/00411457108231440.

[18] A. Walker, P. Mehta, and J. Koller, “Drag coefficient model using the Cercignani-Lampis-Lord gas-surface interaction model,” *Journal of Spacecraft and Rockets*, vol. 51, no. 5, pp. 1544–1563, Sep. 2014, doi: 10.2514/1.A32677.

[19] P. Moore and A. Sowter, “APPLICATION OF A SATELLITE AERODYNAMICS MODEL BASED ON NORMAL AND TANGENTIAL MOMENTUM ACCOMMODATION COEFFICIENTS,” 1991.

[20] Z. Lian, A. Godil, P. L. Rosin, and X. Sun, “A new convexity measurement for 3D meshes,” in *Proceedings of the IEEE Computer Society Conference on Computer Vision and Pattern Recognition*, 2012, pp. 119–126. doi: 10.1109/CVPR.2012.6247666.

[21] X. Jin, F. Huang, X. Cheng, Q. Wang, and B. Wang, “Monte Carlo simulation for aerodynamic coefficients of satellites in Low-Earth Orbit,” *Acta Astronautica*, vol. 160, pp. 222–229, Jul. 2019, doi: 10.1016/j.actaastro.2019.04.012.

[22] J. Bullard, “Satellite Drag Analysis using Direct Simulation Monte Carlo (DSMC),” 2018.

[23] A. de Rooij, “Corrosion in Space,” in *Encyclopedia of Aerospace Engineering*, John Wiley & Sons, Ltd, 2010. doi: 10.1002/9780470686652.eae242.

[24] W. M. Mahmoud, D. Elfiky, S. M. Robaa, M. S. Elnawawy, and S. M. Yousef, “Effect of Atomic Oxygen on LEO CubeSat,” *International Journal of Aeronautical and Space Sciences*, vol. 22, no. 3, pp. 726–733, Jun. 2021, doi: 10.1007/s42405-020-00336-w.

[25] D. Doofing and A. M. M. Finckenor, “Material Selection Guidelines to Limit Atomic Oxygen Effects on Spacecraft Surfaces,” 1999. [Online]. Available: www.sti.nasa.gov

[26] C. R. Stidham, T. J. Stueber, B. A. Banks, J. A. Dever, S. K. Rutledge, and E. J. Bruckner, “Low Earth Orbital Atomic Oxygen Environmental Simulation Facility for Space Materials Evaluation.”

[27] B. A. Banks, K. K. de Groh, and S. K. Miller, “Low Earth Orbital Atomic Oxygen Interactions with Spacecraft Materials,” 2005.

[28] M. Cho, “DISSERTATION EFFECT OF ATOMIC OXYGEN EXPOSURE ON SPACECRAFT CHARGING PROPERTIES SUBMITTED IN PARTIAL FULFILLMENT OF THE REQUIREMENTS FOR THE DEGREE OF DOCTOR OF PHILOSOPHY BY NOOR DANISH AHRAR MUNDARI SUPERVISED BY,” 2011.

[29] B. A. Banks, “Atomic Oxygen Protection of Materials in Low Earth Orbit,” 2002. [Online]. Available: www.sti.nasa.gov

[30] B. A. Banks, J. A. Backus, M. v Manno, D. L. Waters, K. C. Cameron, and K. K. de Groh, “Atomic Oxygen Erosion Yield Prediction for Spacecraft Polymers in Low Earth Orbit,” 2009. [Online]. Available: http://www.sti.nasa.gov

[31] Panagiota Nazlidou “Aerodynamic forces modeling review for Very Low Earth Orbits”, February 2022